Benchmarking laminar fMRI

NeuroImage 197 (2019) 806–817

Contents lists available at ScienceDirect

NeuroImage

journal homepage: www.elsevier.com/locate/neuroimage

Benchmarking laminar fMRI: Neuronal spiking and synaptic activity during top-down and bottom-up processing in the different layers of cortex

Matthew W. Self [a,*], Timo van Kerkoerle [b], Rainer Goebel [c,d], Pieter R. Roelfsema [a,e,f]

[a] Department of Vision & Cognition, Netherlands Institute for Neuroscience, Meibergdreef 47, 1105 BA, Amsterdam, The Netherlands
[b] Cognitive Neuroimaging Unit CEA DSV/I2BM, INSERM, Université Paris-Sud, Université Paris-Saclay, NeuroSpin Center, Gif/Yvette, 91191, France
[c] Cognitive Neuroscience Department, Faculty of Psychology and Neuroscience, Maastricht University, Oxfordlaan 55, 6229 EV, Maastricht, The Netherlands
[d] Department of Neuroimaging & Neuromodeling, Netherlands Institute for Neuroscience, Meibergdreef 47, 1105 BA, Amsterdam, The Netherlands
[e] Department of Integrative Neurophysiology, Center for Neurogenomics and Cognitive Research, VU University, De Boelelaan 1085, 1081HV, Amsterdam, The Netherlands
[f] Psychiatry Department, Academic Medical Center, Postbus 22660, 1100DD, Amsterdam, The Netherlands

ARTICLE INFO

Keywords:
Cortical layers
Spontaneous activity
Feedforward processing
Feedback processing
fMRI
Laminar fMRI
Perceptual organization
Attention
BOLD
Layers
Area V1

ABSTRACT

High resolution laminar fMRI is beginning to probe responses in the different layers of cortex. What can we expect this exciting new technique to discover about cortical processing and how can we verify that it is producing an accurate picture of the underlying laminar differences in neural processing? This review will address our knowledge of laminar cortical circuitry gained from electrophysiological studies in macaque monkeys with a focus on the primary visual cortex, as this area has been most often targeted in both laminar electrophysiological and fMRI studies. We will review how recent studies are attempting to verify the accuracy of laminar fMRI by recreating the known laminar profiles of various neural tuning properties. Furthermore, we will examine how feedforward and feedback-related neural processes engage different cortical layers, producing canonical patterns of spiking and synaptic activity as estimated by the analysis of current-source density. These results provide a benchmark for recent studies aiming to examine the profiles of bottom-up and top-down processes with laminar fMRI. Finally, we will highlight particularly useful paradigms and approaches which may help us to understand processing in the different layers of the human cerebral cortex.

1. Introduction

The spatial resolution of functional magnetic resonance imaging (fMRI) has now reached the level that inferences can be made about the blood oxygen level dependent (BOLD) signal in different laminar compartments of cortex. While several technical challenges remain, it is becoming possible to study layer specific computations in the human cortex. In this review we will examine what we know about the functioning of the different layers of neocortex and the different computations that are performed in these layers. We will focus on the primary visual cortex (area V1) as this has been the most heavily-studied area and exhibits clear differences in laminar processing, though we will also discuss the likelihood that findings from this area can be applied to higher visual areas, or neocortex in general. The six-layered structure of mammalian neocortex is remarkably well preserved, both across species and throughout the brain. With only minor variations in macroscopic laminar architecture between areas, the cortex can implement a huge range of different neural algorithms. In this review, we will highlight those processing differences between the cortical layers of macaque monkeys that are most relevant for studies that aim to use fMRI to study activity in the different layers of the human cerebral cortex. The laminar profiles of spiking and synaptic activity in monkeys can be used as benchmarks to compare to laminar BOLD profiles.

2. Connectivity of the different layers of V1

We have a reasonably detailed understanding of the anatomical inputs and outputs of the different cortical layers of cats and monkeys (Douglas and Martin, 2004; Felleman and Van Essen, 1991; Salin and Bullier, 1995), particularly in the primary visual cortex. The detailed anatomy of the different layers of cortex are reviewed elsewhere in this issue, here we will briefly outline the main connection pathways of V1 (Fig. 1A). In broad terms, layer 4c and layer 6 receive the majority of the direct input from the lateral geniculate nucleus of the thalamus (LGN) (Hendrickson et al., 1978; Hubel and Wiesel, 1968), with some input into layer 2 and 3 as well. The input layer is pathway specific as parvocellular

* Corresponding author.
E-mail address: m.self@nin.knaw.nl (M.W. Self).

http://dx.doi.org/10.1016/j.neuroimage.2017.06.045
Received 20 March 2017; Received in revised form 2 June 2017; Accepted 20 June 2017
Available online 23 June 2017

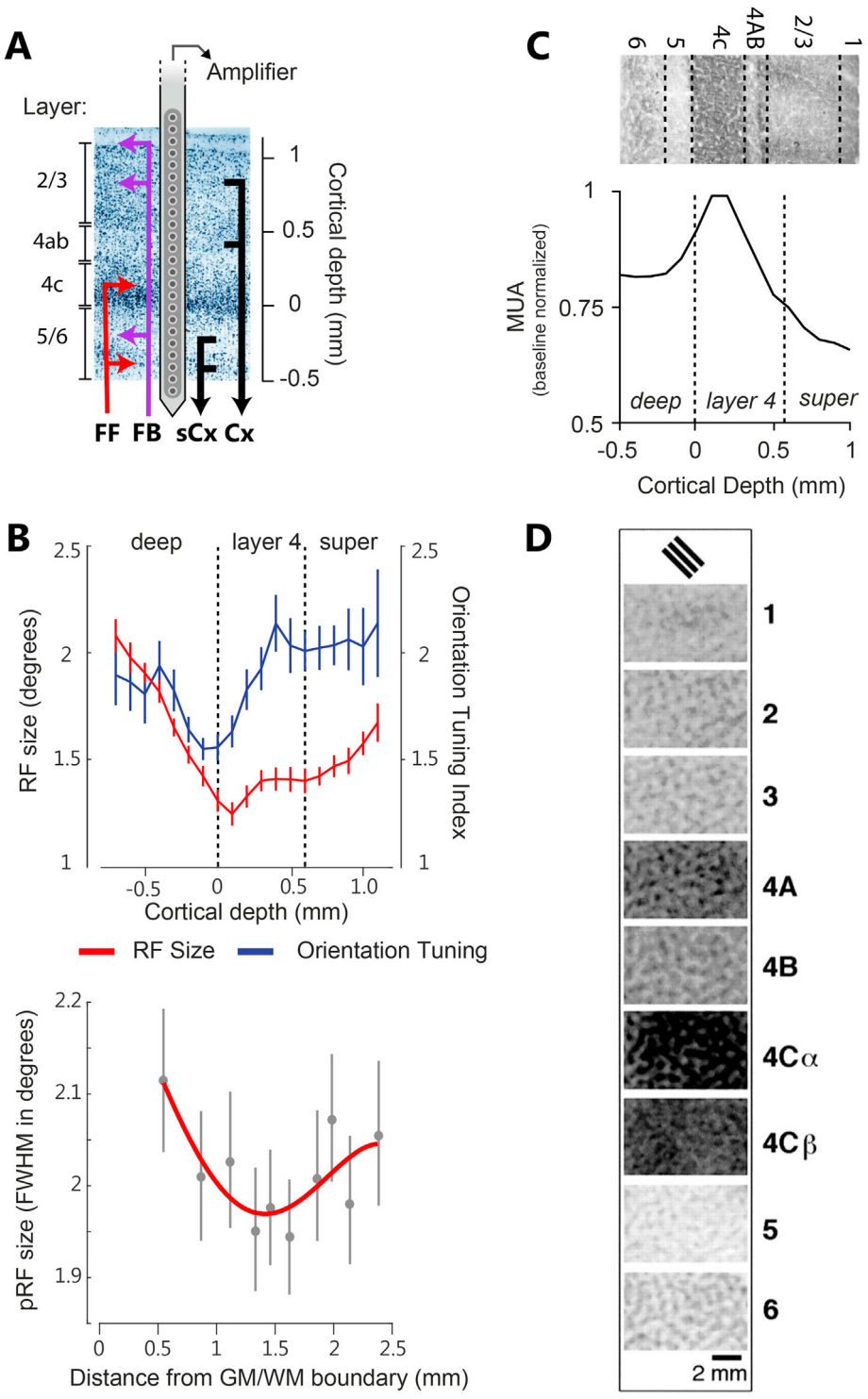

Fig. 1. The laminar organization of cortex. **A)** A Nissl stain from area V1. V1 receives feedforward input from the retina primarily in layers 4c and 6 (red arrows) and feedback from other cortical areas and the pulvinar into layers 1, 2/3 and 5 (purple arrows). Layers 2/3 and 4B provide output to higher cortical areas (arrows marked Cx) and layers 5 and 6 project to sub-cortical regions (arrows marked sCx). Also depicted is a laminar electrode with vertically spaced contacts which can record neural activity simultaneously from each cortical layer. **B)** (Upper panel) The laminar profiles of orientation tuning strength (blue line) and receptive field size (red line) recorded in macaque area V1 using laminar electrodes. RFs were measured using a moving oriented bar across a grey screen, see (Self et al., 2013) for further details. Orientation tuning indices (OTI) were calculated as the response to the preferred orientation of the bar divided by the response to the least preferred orientation. Higher numbers correspond to stronger orientation tuning. Errors bars, ±1 s.e.m. (Lower panel) Laminar fMRI data taken from Fracasso et al. (2016) showing the size of population receptive fields at different cortical depths. The error-bars show 95% confidence intervals. **C)** The laminar profile of spontaneous multi-unit activity (MUAe) in V1 from two macaque monkeys. The data come from the last 150 ms of a pre-stimulus baseline period, in total 300 ms in duration, while the monkeys fixated on a dot present on an otherwise grey screen. Multi-unit activity from each layer was normalized to the layer with the strongest activity, which was always in layer 4c. The normalized profile was then averaged across penetrations. The panel above shows the pattern of staining for cytochrome oxidase from V1 taken from Lund (1988). **D)** The laminar profile of DG uptake from the primary visual cortex of a macaque monkey taken from Vanduffel et al. (2000) showing stronger visually-related metabolic activity in layer 4c.

LGN axons target layer 4cβ whereas magnocellular projections target 4cα. The less numerous koniocellular projections target the superficial layers and not layer 4 (Klein et al., 2016). The deep layers (layers 5 and 6) send projections to sub-cortical structures, layer 5 to the superior

colliculus and layer 6 to the LGN (Blasdel and Lund, 1983; Lund, 1988). The superficial layers (2 and 3) (Livingstone and Hubel, 1984) and layer 4B (Maunsell and van Essen, 1983) send projections to other cortical areas and layer 1 is a cell-sparse layer which receives a large amount of feedback from other cortical areas (Anderson and Martin, 2009; Rockland and Virga, 1989) and the pulvinar nucleus of the thalamus (Benevento and Rezak, 1975; Ogren and Hendrickson, 1977). These layers are strongly interconnected via intracolumnar connections that form the cortical micro-circuit (Binzegger et al., 2004; Callaway, 2004) and the superficial layers and layer 5 also send connections horizontally to neurons in the same layers representing nearby regions of the retina (Gilbert, 1983; Rockland and Pandya, 1979).

3. Methodological issues in laminar electrophysiology and fMRI

Despite the relatively detailed understanding of the connectivity of cells in different layers, our understanding of the function of these layers remains limited. Early studies investigated laminar processing using single metal electrodes that were slowly advanced through the layers to record spiking-activity from single cells sequentially in different layers (Gilbert, 1977; Hubel and Wiesel, 1962). These studies predominantly emphasized the similarities between tuning properties across the different laminae, leading to the concept of the cortical column, but they also revealed some differences in the tuning properties of cells in different layers of cortex (reviewed below). More modern studies typically use multi-contact electrodes to record activity from each layer of cortex simultaneously (Fig. 1A). These electrodes allow researchers to construct laminar profiles of the strength of neural activity as well as the calculation of current source density (CSD), which can be used under certain assumptions to estimate synaptic inputs to the different layers (Mitzdorf, 1985). These profiles of activity in the different layers of experimental animals can be compared to the activity profiles obtained using BOLD fMRI in humans.

The comparison between spiking and synaptic activity in the different layers of monkeys and laminar fMRI is complicated by many issues. Firstly, the relationship between the BOLD signal and neural activity is still unclear. It appears that many different forms of neural activity correlate with the BOLD signal, with each form of activity giving a slightly different view of laminar processing. Here we will focus on studies of spiking activity and LFP/CSD (see below), whereas the companion article from the Fries group reviews studies of oscillatory activity in different layers. The laminar profile of the BOLD signal is complicated by the fact that GE fMRI is most sensitive to signals from large blood vessels so that the fMRI signal is biased towards the large veins on the pial surface. Furthermore, as the blood drains from the lower to higher layers, the signal in the upper layers may contain a mix of signals from lower layers. This can lead to a smearing out of tuned responses, for example the small blood vessels in the parenchyma of V1 of the cat are tuned for orientation whereas the large pial veins are untuned as they collect blood from many different orientation columns (O'Herron et al., 2016). These effects lead to a general increase in the amplitude of GE BOLD signals towards the superficial layers, and a reduction in the specificity of the response in these layers, which may obscure the underlying laminar profiles. Previous studies have combatted this issue either by masking out the signal from the pial veins (Chen et al., 2013; Koopmans et al., 2010) or by using a spatial general linear model approach to estimate the unique contribution of each layer (Kok et al., 2016). Other studies have avoided this issue by using spin-echo (SE) weighted (Goense and Logothetis, 2006) or combined GE/SE sequences (De Martino et al., 2013) which are more sensitive to smaller vessels at the cost of reduced signal-to-noise ratios. In addition, the density of the microvasculature is not uniform across the different layers, with the highest capillary densities in V1 being found in layer 4c (Weber et al., 2008). This factor could act to bias the BOLD signal towards the middle layers and may complicate comparisons with neural activity profiles.

Laminar fMRI also pushes the limits of the spatial resolution of GE BOLD, which is currently approximately 0.8 mm^3, though this may be improved upon in the future. At this resolution, the size of an individual voxel is larger than the size of some layers leading to partial volume effects in which a voxel contains signals from multiple layers. This issue is compounded by the fact that cortical thickness varies according to the folding of cortex; cortex is thinner in the fundus of a sulcus and thicker at the crown of a gyrus and the relative thicknesses of the different layers varies with curvature. The superficial layers are thicker in the fundi of sulci and the deeper layers are thicker on the crowns of gyri. This makes averaging across voxels sitting in sulci and gyri more complex and sophisticated analysis approaches must be used (Kemper et al., 2017; Zimmermann et al., 2011).

The complications inherent in producing laminar profiles of BOLD responses mean that it is imperative to compare the results to known laminar profiles from the electrophysiological literature. It is clear from electrophysiological studies that laminar activity profiles vary depending on the circuits that they engage. Spontaneous activity, visually driven activity and sustained visual activity all have different laminar profiles. Most notably, stimuli/tasks that strongly recruit feedback projections from higher visual areas produce different laminar profiles of neural activity in V1 compared to those that do not. We will review these different processing modes and compare the electrophysiological data to recent fMRI studies that have examined laminar BOLD signals in humans.

4. Laminar differences in the tunings of neurons

Cells in macaque primary visual cortex (V1) are strongly tuned for several visual features. These cells typically prefer a visual stimulus in a particular position on the retina (their receptive field, RF) with a particular size, orientation, spatial frequency and eye of origin. These tuning properties vary from cell-to-cell in well-organized maps such as the familiar retinotopic maps which can be revealed using fMRI (Engel et al., 1994; Wandell et al., 2007). Some of these maps vary little across the different layers of V1. Hubel and Wiesel demonstrated that cells in V1 are organized into functional columns which have similar preferred stimuli at all depths, such as the famous orientation tuning columns (Hubel and Wiesel, 1962). Nevertheless, some tuning properties do show considerable variation across the layers and hence form characteristic laminar profiles. For example, orientation tuning strength is not uniform across the layers. In the classical view, the stellate cells of layer 4c and cells in the cytochrome oxidase 'blobs' of layer 2/3 are largely non-orientation tuned (Livingstone and Hubel, 1984) whereas the majority of cells in all other layers are strongly tuned for orientation. More recent studies suggest a wide variety of orientation tuning strengths in different layers (Ringach et al., 2002) with weaker tunings in layer 5 and layer 4c. We were recently able to confirm this view using a laminar electrode which allows simultaneous recordings from each layer of cortex (Self et al., 2013). Multi-unit orientation tuning strength was weakest at the boundary of layer 5 and layer 4c, producing a characteristic laminar profile (Fig. 1B).

Receptive field size also varies across the layers. Cells in layer 4c have the smallest RFs and RFs get progressively larger as one moves to deeper or shallower depths, with RF sizes in layer 6 being particularly large (Fig. 1B) (Gilbert, 1977; Hubel and Wiesel, 1977, 1968; Schiller et al., 1976; Self et al., 2013) although not all studies agree (Sceniak et al., 2001; Snodderly and Gur, 1995). Eye dominance is also highly organized across depth: most cells in layer 4c of the monkey are monocular whereas cells in the superficial layers receive input from both eyes in varying degrees according to their position on the ocular dominance map (Hubel and Wiesel, 1969, 1968). Measuring these laminar profiles using fMRI provides a useful means to verify the accuracy of the technique, as tuning properties can be accurately measured using a wide-range of signal intensities, and therefore this technique does not suffer from the variations in BOLD signal magnitude across the different layers of cortex. A recent study used population receptive field (pRF) mapping techniques to

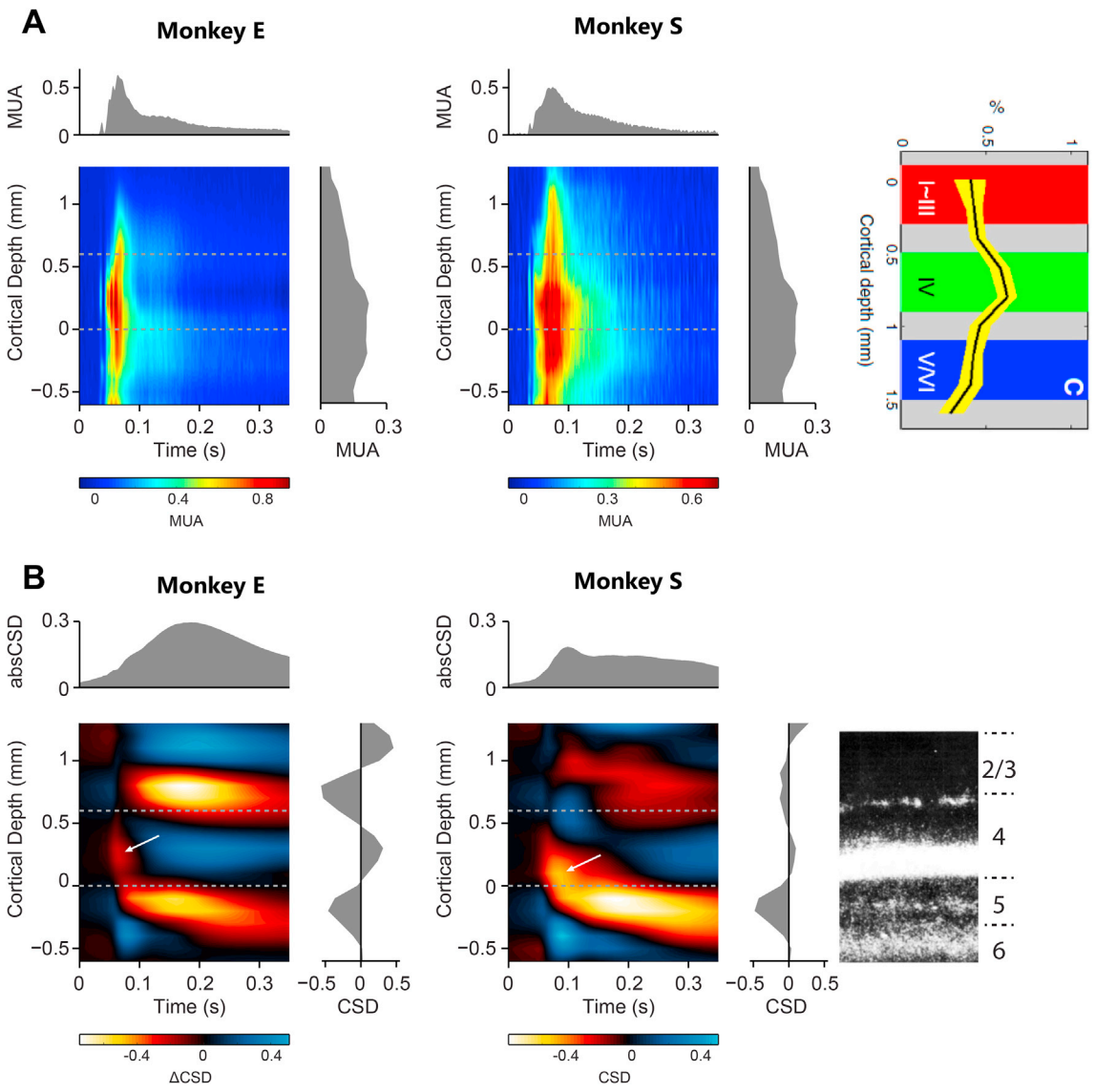

Fig. 2. The laminar profile of visually driven activity. A) The color panels show MUAe activity from V1 of two monkeys in response to the presentation of a full-screen texture. Warmer colors denote stronger spiking activity. The small initial peak shows the input arriving from the LGN. The graph on top shows the average response across the layers, while the graph to the right shows the laminar profile obtained from averaging over time (0–350 ms after stimulus onset). The laminar profile peaks at the boundary between layer 4c and layer 5. For comparison, the panel to the right shows the laminar profile of visually driven BOLD activity taken from Chen et al. (2013). **B)** Current source density responses to the same stimuli as above. The visual stimulus triggers an initial sink in layer 4c (arrow) followed by more sustained sinks in layer 5 and layer 2/3. The laminar profile (graph on the right) was constructed by averaging the CSD over time (100–350 ms after stimulus onset). The graph on the top illustrates the average absolute value of the CSD across layers. The panel on the far right shows an autoradiograph of V1 after injections of radioactive tracers in the LGN, revealing the pattern of feedforward projections from the LGN to V1 (Hendrickson et al., 1978).

measure the laminar profile of RF size in human V1 (Fracasso et al., 2016). The resulting profile was similar to that derived from multi-unit activity measured in macaque V1 (Self et al., 2013) (Fig. 1B), although the differences between layers were much more apparent in the electrophysiological data. This difference is likely due to partial-volume effects; due to the large size of individual voxels, signals from multiple layers will often contribute to the response of a single voxel. This effect will unavoidably reduce the differences between layers in BOLD studies. Nevertheless, this study's use of a model-based approach points the way to future studies which could examine how neuronal activity in the different layers is influenced by visual context, behavioral state, task learning, development and disease.

5. Laminar differences in spontaneous activity

The basic metabolic activity of neurons in the different cortical layers have been measured in experiments looking at the level of uptake of radioactively labelled 2-deoxyglucose (DG). Cells which are highly metabolically active will take up more DG than less active cells and they will therefore appear to be darker on post-mortem autoradiographs. Studies of DG uptake in the primary visual cortex of monkeys have shown that there is little variation in the laminar uptake of DG if an animal is binocularly deprived of visual input (Kennedy et al., 1976), however this may be a rather unnatural situation as the visual cortices may be actively suppressed in these cases. Indeed, if an animal is shown a uniform grey screen then a characteristic laminar profile of DG uptake develops with the highest uptake in the input layers: layer 4c and layer 6 (in that order) (Tootell et al., 1988a). These laminar patterns of metabolic activity correspond well to the pattern of staining obtained for the mitochondrial enzyme cytochrome oxidase (Horton and Hubel, 1981; Wong-Riley, 1979) suggesting that metabolic activity varies across the layers, being highest in layer 4c (Fig. 1C, top). Does this variation in metabolic activity

reflect different levels of spontaneous neural activity? A study using a single-electrode that was lowered through cortex, making a series of recordings from cells at different depths, suggested that spontaneous activity was indeed highest in layer 4c, 4A and layer 6 (Snodderly and Gur, 1995). In this study, the authors listened for regions along the electrode trajectory in which multi-unit 'background' activity was strong. These regions coincided well with the ex-vivo staining for cytochrome oxidase. They also recorded from single-cells along the trajectory and found that the highest spontaneous spike-rates were found in the input layers 4 and 6 (see also Ringach et al., 2002). It is, however, difficult to construct profiles of activity using a single electrode, as activity in different layers is recorded at different time-points and the depth of the electrode has to be assessed using histological techniques ex vivo.

Using a multi-contact electrode, it is possible to simultaneously measure activity levels across the cortical layers, although is often difficult to isolate single neurons in all layers simultaneously. One solution is to create an estimate of the laminar profile of spiking activity by using the envelope of multi-unit activity (MUAe) (Supèr and Roelfsema, 2005; Xing et al., 2009). This signal measures the signal power in the high-frequency spiking range (typically 500 Hz–5000 Hz). It has some advantages for comparisons with fMRI results over traditional SUA/MUA measurements because it constitutes an average of the local spiking activity within 50–150 microns of the electrode contact. Traditional techniques are biased towards sampling from neurons with the largest spikes and the contributions of small amplitude spikes are largely ignored. MUAe may therefore give a better estimate of the overall level of spiking in a particular layer. Recordings from awake monkeys during the baseline period of a visual task show that the pattern of spontaneous MUAe strongly resembles the metabolic and spike-rate data with the strongest signals in layer 4c and weaker signals as one moves away from this layer (Fig. 1C). The metabolic and electrophysiological data predict that the highest amplitude BOLD signals should be found in layer 4. Furthermore the density of the microvasculature is highest in this layer (Duvernoy et al., 1981). However, it is difficult to measure a profile of spontaneous activity using the BOLD signal as this does not provide an absolute signal. Future studies measuring blood flow may be useful for examining the laminar profile of spontaneous activity in humans.

6. The laminar profile of visually driven activity

The presentation of a visual stimulus causes a dramatic rise in metabolic, spiking and synaptic activity in the visual cortex. DG studies have shown highly spatially specific increases in DG uptake at the locations in V1 corresponding to the location of the visual stimulus (Tootell et al., 1988b; Vanduffel et al., 2000). Metabolic activity varies across the layers, being strongest in layer 4C, 4A and layer 6 (Fig. 1D). Electrophysiological studies of V1 in macaques have examined laminar activity profiles using a wide array of visual stimuli, ranging from low-spatial frequency stimuli (Maier et al., 2011; Schroeder et al., 1998, 1991; Xing et al., 2014), high-contrast drifting gratings (Xing et al., 2012), textures (Self et al., 2013) and line segments (van Kerkoerle et al., 2017). These studies have also focused on different aspects of spiking and synaptic activity.

Pioneering studies using multi-contact electrodes found the strongest multi-unit spiking activity in layer 4c (Schroeder et al., 1998, 1991). These studies used diffuse light as a stimulus which activates the non-orientation tuned cells of layer 4c cells, but it might be suboptimal for the orientation-tuned cells in the extragranular layers. Spiking activity profiles from these studies may therefore have been biased towards finding the strongest activity in layer 4c and weaker activity in other layers. A later study using a drifting sine-wave grating as a stimulus (Xing et al., 2012) revealed a much flatter profile of spiking activity with no clear differences between the layers, although layer 2/3 contributed more strongly to the total number of spikes. However, this study used a method of recording multi-unit activity that counts all spikes above a certain threshold, which may be biased towards particularly large spikes. It is therefore of interest to examine the laminar profile of visually driven activity using a method sensitive to all spikes, such as MUAe. Although we have previously published laminar activity profiles of the visually driven MUAe signal (Poort et al., 2016; Self et al., 2013, 2012; van Kerkoerle et al., 2017), for the purposes of the previous studies the signal was normalized to the peak response of the individual recording channels. Such a normalization step removes activity differences between the layers. We here therefore recomputed the activity profiles across the layers but we now omitted the normalization step. Fig. 2A presents non-normalized MUAe laminar profiles in response to oriented texture stimuli. It can be seen that MUAe does have a clear visually driven laminar profile with the highest activity around the boundary of layer 4c and layer 5. Spiking activity becomes weaker at electrode contacts further away from this boundary and activity is weakest in the superficial layers. While the reduced response in the superficial layers compared to the study of Xing et al. (2012) may be partially due to the use of full-screen stimuli which induce stronger levels of surround suppression in these layers, a similar laminar profile was observed in other monkeys viewing different stimuli including high-contrast checkerboards and thin line-segments (van Kerkoerle et al., 2017), suggesting that it may represent a canonical laminar profile of visually driven activity. It should be noted, however, that very different visual stimuli, such as the luminance stimuli used in Schroeder et al. (1998) and Xing et al. (2014), will lead to differences in the laminar profile of spiking activity. Hence, the precise stimulus used to elicit visually driven activity should always be kept in mind when making comparisons with the profiles resulting from laminar fMRI studies.

Do visually driven BOLD activity profiles resemble those presented in Fig. 2A? Studies which have masked out the signals from pial veins (Chen et al., 2013; Koopmans et al., 2010) or that have used spin-echo (SE) weighted (Goense and Logothetis, 2006) or combined GE/SE sequences (De Martino et al., 2013) to increase the sensitivity for smaller vessels have observed greater amplitude BOLD signals in layer 4. This match between the profile of spiking activity and BOLD signal strength across the layers appears promising.

It is important to note, however, that the correlation between spiking and the BOLD signal will not only depend on the visual stimulus, but also on other factors, including the neuro-modulatory tone and the arousal of the animal (Logothetis, 2008). This is because the BOLD signal is thought to be driven by vasodilatory signals which arise primarily through synaptic activity and the release of neuromodulators (Attwell and Iadecola, 2002; Lauritzen, 2005). Often an increase in synaptic activity, and hence vasodilation, will be coupled with an increase of spiking activity. Indeed, studies that have examined the link between synaptic activity, approximated using the local field potential (LFP), and the BOLD signal have generally found that the strength of LFP, multi-unit spiking and the BOLD signals tend to co-vary (Goense and Logothetis, 2008; Logothetis et al., 2001; Mukamel et al., 2005). However, in cases where the level of spiking and the LFP become decoupled from each other (e.g. when using stimuli that produce strong suppression), the BOLD signal more closely follows the LFP (Goense and Logothetis, 2008; Logothetis et al., 2001; Maier et al., 2008; Wilke et al., 2006).

Within the context of this review it is interesting to examine how well the laminar profile of the visually-driven LFP predicts the BOLD signal. The LFP is a complex signal comprising the summation of electric activity over a volume of neural tissue, and the contribution of local and remote sources to the signal is still a matter of debate (Berens et al., 2008; Busse et al., 2011; Kajikawa and Schroeder, 2011; Xing et al., 2009). A useful technique to remove the contribution of remote sources is to compute the one-dimensional current source density profile (CSD), which is proportional to the second spatial derivative of the local field potential (LFP). This derivation of the CSD is only valid if certain assumptions are met, in particular the laminar electrode must be oriented orthogonally to the cortical layers and the activation of the cortical layers must be fairly uniform in the plane of the layers (for more details see Mitzdorf, 1985). The CSD calculation removes global components from the LFP and it

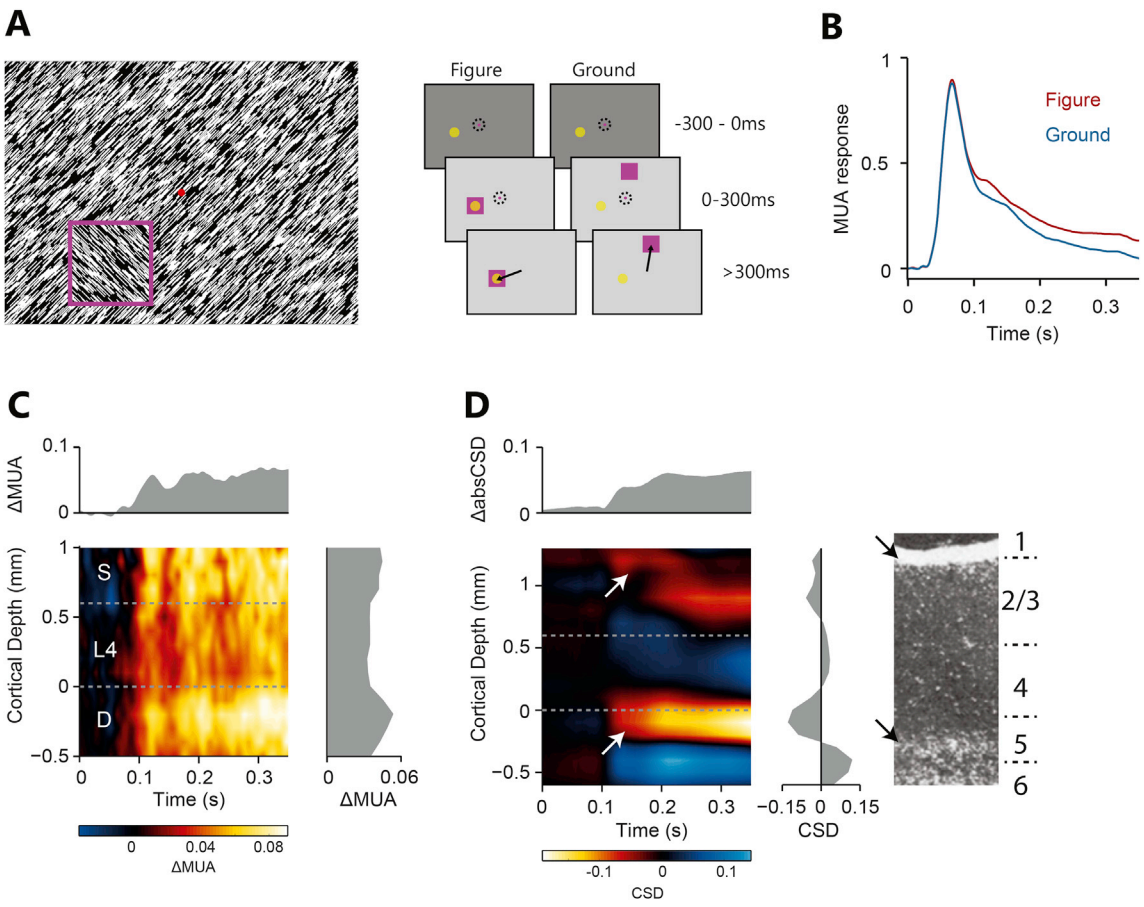

Fig. 3. Figure-ground modulation in the different layers of V1. A) The stimulus used to test figure-ground segregation. The purple outline around the figure was added here for clarity but absent in the experiment. The panels to the right show the behavioral paradigm. The monkey had to fixate on the red dot, the texture appeared and the animal was required to make a saccade to the figure when the fixation dot disappeared. The yellow circle marks the location of the RF. **B)** The average V1 MUAe response across all layers and penetrations from two monkeys showing late (>100 ms) figure-ground modulation. **C)** The difference between figure and ground responses, or figure-ground modulation, across the different layers. Hotter colors equal stronger modulation. The laminar profile to the right shows stronger modulation in layer 5 and the superficial layers (100–350 ms after stimulus onset). **D)** The difference in CSD between figure and ground. Figures produce stronger sinks in layer 5, layer 1 (arrowed) and later in layer 2/3. The panel on the far right shows the projection pattern of feedback axons (light regions) from V2 to V1 taken from Rockland and Pandya (1979). Note the close correspondence between the layers that receive feedback and the layers with enhanced sinks in the presence of a figure (arrows).

reveals the laminar depth of current sinks and sources (Buzsáki et al., 2012; Mitzdorf, 1985; Nicholson and Freeman, 1975). Although the precise contribution of different neural processes to the CSD is still a matter of debate, current sinks occur at the cortical depths where currents flow into neurons and they therefore provide evidence for excitatory post-synaptic activity, in particular if they coincide with an increase of spiking activity. Current sources occur in the layers where the current passively flows out of the neurons, back into the extracellular medium or at sites of active inhibition. The laminar profile of the CSD may therefore provide a useful link between neurophysiological recordings and the BOLD signal, because both signals are thought to be dominated by synaptic activity.

The CSD response to a strongly driving visual stimulus (e.g. a full-screen checkerboard) has a characteristic spatiotemporal profile across the layers of V1. The presentation of the stimulus triggers a wave of visual input arriving from the thalamus, which gives rise to a current sink in layer 4c (Fig. 2B). This sink is extremely reliable, and once layer 4c has been located it can be used to assign the different sites of a laminar electrode to all the layers on the basis of the known layer thicknesses. Once the initial sinks and sources elicited by the onset of the visual stimulus subside, a more sustained CSD pattern emerges with strong sinks in layers 2/3 and 5/6 (Maier et al., 2011; van Kerkoerle et al., 2014). This suggests that, once the initial visual transient subsides, strong synaptic activity occurs in the agranular layers.

The laminar CSD profile in response to visual stimulation, with strong sustained sinks in layers 2/3 and 5/6, therefore appears to differ from the BOLD profile, which peaks in layer 4. Hence, in spite of previous results indicating that the BOLD signal correlates better with LFP-markers than with spiking activity, the somewhat paradoxical finding is that the laminar profile of the visually-driven BOLD signal corresponds better to that of spiking activity. We wish to add a note of caution here however, as this finding may depend on the exact visual stimulation used, and the lack of studies that have simultaneously measured CSD and fMRI makes it difficult to draw conclusive comparisons. Ultimately, future work comparing these signals is needed to further our understanding of the link between visually-driven neural activity in different layers and the laminar BOLD signal.

7. Top-down modulation of neuronal activity in the different cortical layers

Feedforward projections from the lateral geniculate nucleus of the thalamus (LGN) and feedback projections from higher cortical areas terminate in largely separate zones in V1. The predominant target layers for afferent axons from the LGN are layer 4c and layer 6, as was described above. In contrast, feedback projections from higher cortical areas back to area V1 tend to avoid layer 4 (Felleman and Van Essen, 1991). The exact laminar targets for feedback axons depends on the source area of the feedback. However, over 90% of the feedback that V1 receives comes from V2 (Markov et al., 2014) and these axons target layer 1 with

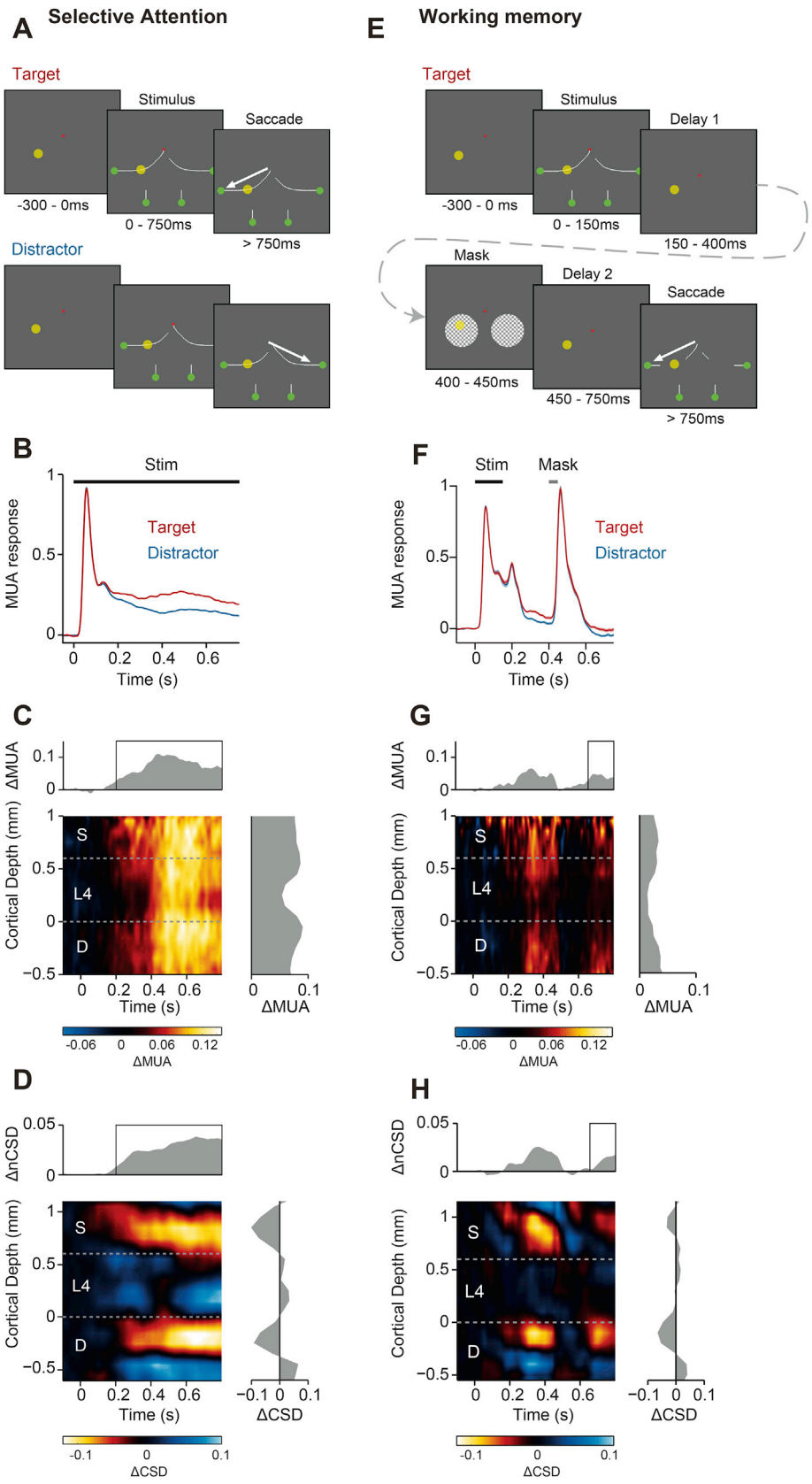

Fig. 4. The laminar profile of attentional modulation and working memory related activity. A) Illustration of the curve-tracing task. The animal fixates the red dot. The curves appear and the animal mentally traces the curve that is connected to the fixation point. When the fixation point disappears the animal makes a saccade to the green circle connected to the fixation point. The RF can either be on the target curve (left panels) or one of the distracter curves (right panels). **B)** The response averaged across the layers in V1 of two monkeys. Spiking activity elicited by the target curve (red) is stronger than that elicited by the distractor (blue). **C)** The difference in MUAe between the target and distracter in the layers of V1. The graph on top shows the average across layers, with the small box indicating the time window used to calculate the laminar profile depicted on the right. The laminar profile shows a 'U' shape, with stronger modulation in layer 5, upper layer 4 and the superficial layers and weaker modulation in layers 4c and 6. **D)** The CSD difference between target and distracter. Attentional

collateral branches targeting layers 2 and 5 (Anderson and Martin, 2009; Rockland and Pandya, 1979; Rockland and Virga, 1989). This unique anatomical profile could provide a useful marker for feedback-related processes in human visual cortex, if it also translates into a functional segregation of activity in the different layers.

We have recently studied the contribution of feedback projections to activity across the cortical layers in a number of tasks that engage top-down projections back to the primary visual cortex. In one set of studies, monkeys performed a texture segmentation task in which they had to report the location of a small texture-defined figure located on a background texture composed of thousands of oriented lines (Fig. 3A). The figure can be placed in the RF of the cells under study or it can be situated outside the RF so that responses to the background can be recorded (Fig. 3A, **right**). Neural activity in V1 shows two clear phases during this task (Fig. 3B). The initial response (50–100 ms after stimulus onset) is driven by the feedforward input from the LGN and it depends upon the orientation of the lines in the RF. In this early phase, there are no differences between the neuronal responses elicited by the figure and the background. At a later time-points (>100 ms) responses become modulated by the visual context (Lamme, 1995) (Fig. 3C). The figure elicits extra spiking activity whereas the activity elicited by the background is suppressed (Poort et al., 2016). This difference in spiking activity is known as figure-ground modulation (FGM) and it is thought to arise through feedback from higher visual areas because FGM is weaker if the animal does not attend the figure (Poort et al., 2012) and it is suppressed by anesthesia (Lamme et al., 1998). When we examined the laminar profile of FGM, we found that it was weakest in layer 4 and higher in the superficial and deep layers (Poort et al., 2016; Self et al., 2013) creating a 'U' shaped profile (Fig. 3C). The modulation of spiking was accompanied by changes in the CSD pattern. Figures produced extra current sinks in the superficial layers and layer 5 at the same time that the spiking increased in this condition (Fig. 3D). These layers are the primary targets for feedback axons from higher visual areas, especially area V2, suggesting that CSD may be a sensitive measure of the laminar location of the synapses which cause figure-ground modulation. It should be noted however that these layers are also the targets of connections from the pulvinar nucleus of the thalamus (Benevento and Rezak, 1976; Gambino et al., 2014; Shipp, 2003). Thus, the extra spiking activity elicited by figures and their characteristic CSD pattern could originate from feedback from higher cortical areas, from higher order thalamic nuclei or from both (Sherman, 2016). Hence, further work is required to investigate the precise circuit mechanisms of figure-ground segregation.

In another study (van Kerkoerle et al., 2017) we examined responses across the layers of V1 while monkeys performed a curve-tracing task (Roelfsema et al., 1998). In this task the monkey mentally traces a curve that is connected to the fixation point and ignores a distractor curve (Fig. 4A). The animal reports which curve is connected by making a saccade to a green circle at the end of the connected curve. Previous studies have shown that object-based attention gradually spreads along the target curve, highlighting all the contours of the target curve with attention (Houtkamp et al., 2003; Scholte et al., 2001). This spread of object-based attention is associated with enhanced neuronal activity in V1 along the target curve, with a latency that depends on the distance of the RF from the start of the curve, suggesting that the extra spiking activity gradually spreads along the target curve (Fig. 4B) (Pooresmaeili and Roelfsema, 2014; Roelfsema, 2006). Fig. 4B illustrates how the initial V1 response, driven by bottom-up input from the LGN, does not discriminate between target and distractor curve. However, at a later point in time, the mental tracing process causes an increase in spiking activity for the target curve (red in Fig. 4B). When we examined the laminar profile of the attentional modulation of spiking activity, we found it to be weakest in layer 4c and it formed a U-shaped profile similar to that observed in the texture segmentation task (Fig. 4C). The enhanced spiking activity elicited by the target curve was accompanied by sustained increased sinks in layer 5 and the superficial layers in the CSD (Fig. 4D), which suggests that there is additional synaptic input in the layers that are targeted by feedback connections.

The study by van Kerkoerle et al. (2017) also investigated the neuronal correlates of working memory across the layers. The stimulus contained three branching points: at the fixation point, the target curve either branched into the left or right hemifield and there were two additional branching points where the target curve could either turn laterally or downward (Fig. 4E). To probe the animals' working memory, we presented the stimulus only briefly and we then presented a mask at both peripheral branching points. At the end of the trial, part of the stimulus reappeared, but we did not present the contour elements at the peripheral branching points, which the animals also had to maintain in working memory (Fig. 4E). In the first delay, before the mask appeared, neuronal activity elicited by the memory of the target curve was stronger than the activity that was elicited by the memory of the distractor (150–400 ms in Fig. 4F). The appearance of the mask caused a strong burst of spiking in V1, which erased the difference between the memory trace of the target and distractor curves (Fig. 4F and G). After the mask was removed, however, the memory for the target curve again elicited increased V1 activity (after 600 ms in Fig. 4F), demonstrating a neuronal correlate of working memory in the primary visual cortex. The laminar profile of the enhanced spiking activity was similar to that when the stimulus remained visible (compare Fig. 4C and G), but the overall enhancement of spiking activity was less in the memory condition. The CSD profile of working memory for a contour element strongly resembled the profile during attentional modulation (Fig. 4H). The result suggests that a working memory trace of the curve was maintained in brain areas that were not susceptible to the mask, and that these areas reinstated activity in V1 using top-down projections after the mask was removed. This reinstatement provides a measure of top-down effects in the absence of visual stimulation, as the visual stimulus had been absent for several hundred milliseconds by the time the activity was reinstated.

Taken together, the results from the figure-ground segregation, curve-tracing and working memory paradigms, which all appear to rely on feedback connections, show a highly consistent pattern of both modulation of spiking activity and CSD profiles across the layers. The striking similarity suggests a canonical laminar profile of neural activity across the layers of V1 for different stages of neural processing (Fig. 5). If there is no stimulus on the screen, baseline levels of activity are higher in layer 4c (particularly) and layer 6 than in the other layers (Fig. 5A). The onset of the visual stimulus produces a wave of synaptic input arriving in layer 4c which produces strong spiking peaking at the layer 4/layer 5 boundary and becoming weaker further away from this boundary (Fig. 5B). At later time-points, V1 receives top-down input from higher areas and/or the pulvinar which targets the upper layers (1–2) and layer 5 leading to stronger spiking across the superficial and deep layers for the (memory of) image elements that matter for behavior (Fig. 5C). Further studies will be needed to verify how general these profiles are across tasks and across brain areas. One previous study found stronger attentional modulation of the CSD in the extragranular layers in V1 and V2 (Mehta et al., 2000), in broad agreement with the top-down profile.

modulation causes strong and sustained sinks in layer 5 and the superficial layers. The graph on top shows the average of the absolute CSD over layers and the graph on the right the average across time. **E)** The working memory paradigm. The animal performs the curve-tracing task, but now the stimuli disappear from the screen and are masked. A partial version of the stimulus is shown at the end, without information about the correct choice at the more peripheral bifurcation, so that the monkey has to recall the correct target from memory. **F)** Average MUAe responses in V1 of two monkeys. The mask abolishes the working memory effect (difference between the memory for the target and distractor) but it is later reinstated. **G)** The laminar profile of the memory-modulation, same conventions as in panel C. **H)** The difference in CSD between the target and distracter, same conventions as in panel D. The reinstatement of the memory modulation after the mask is associated with a pattern of sinks in layers 1, 2/3 and 5 that strongly resembles the initial pattern.

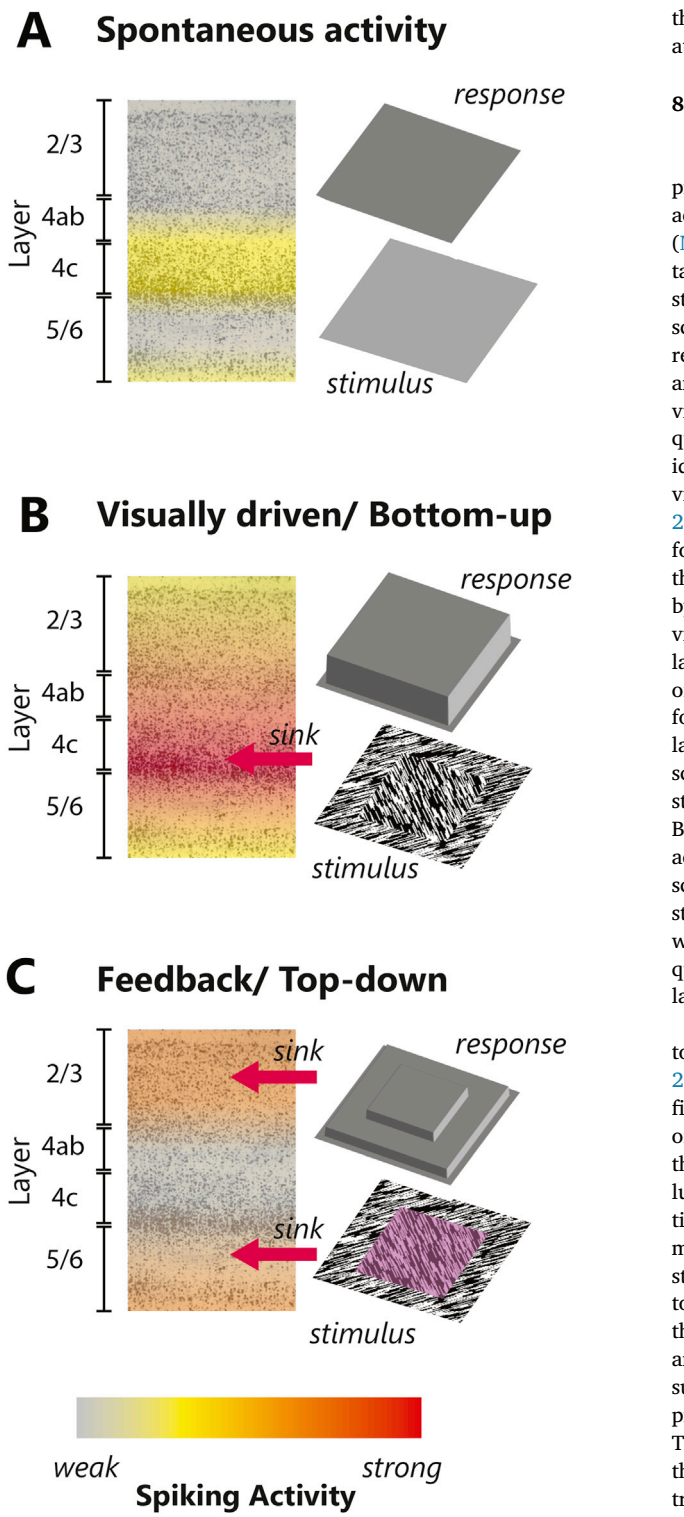

Fig. 5. Canonical laminar profiles for different neural processes in V1. A) Spontaneous spiking activity (grey screen) is strongest in layer 4 and (to a lesser degree) layer 6. **B)** The presentation of a visual stimulus (here a textured stimulus), leads to strong spiking that peaks at the boundary of layer 4c and layer 5. The first sink in the CSD profile appears in layer 4c (arrow). **C)** The region defined by the figure receives top-down projections from higher areas that target the superficial and layer 5 leading to sustained sinks in these layers (arrows), causing enhanced spiking in the superficial and deep layers and a weaker effect in layer 4c.

Interestingly, a recent study of the laminar profile of attentional modulation in mid-level area V4 found that the strongest effects of attention on spiking activity occur in layer 4 (Nandy et al., 2017). This result suggests that the laminar profile of top-down processing may differ between areas at the successive stages of the visual cortical hierarchy.

8. Laminar fMRI studies of top-down effects

Laminar MRI studies that have examined the BOLD activity profiles produced by top-down projections have focused on contextually induced activity patterns, in the absence of bottom-up stimulation. In one study (Muckli et al., 2015) subjects were presented with natural scenes containing a blanked-out (occluded) region (Fig. 6A). The authors of the study showed previously that it is possible to decode the identity of the scene from the BOLD activity in parts of V1 representing the blanked-out region (Smith and Muckli, 2010). Because this region does not receive any feedforward input it suggests that feedback from higher areas provides information about scene identity information to V1. In the subsequent study, the authors examined the ability to decode the scene identity from the BOLD signal at different laminar depths of the early visual cortex, using multi-voxel pattern analysis techniques (Muckli et al., 2015). Decoding accuracy for the non-stimulated parts of V1 was highest for signals derived from the most superficial layers (Fig. 6B). As expected, the decoding accuracy for the regions of V1 that were directly stimulated by the scene was higher than that for the blanked-out region, but at these visually driven locations decoding accuracy was fairly uniform across the layers. This finding partially agrees with the electrophysiological studies of top-down influences and working memory described above which found strong modulations of spiking and CSD in the superficial layers and layer 5, although the BOLD study did not find evidence for increased scene information in layer 5. We note, however, that this laminar fMRI study focused on decoding performance rather than the amplitude of the BOLD signal and the relationship between BOLD amplitude and decoding accuracy is not straightforward. Indeed, the ability to decode the visual scene when it was not occluded by the blank region was relatively constant across layers, while the amplitude of the gradient echo (GE) signal was highest for the superficial layers. It therefore remains an open question whether the lack of significant decoding ability in the deeper layers of V1 was due to the lower signal amplitude in these layers.

Another study examined the activity in the visual cortex in response to illusory Kanisza figures using laminar GE BOLD signals (Kok et al., 2016). Illusory figures (Fig. 6C) allow the study of the representation of figures in the absence of any bottom-up visual drive, because the percept of a figure is induced by remote 'pac-man' shapes. The authors examined the modulatory signal on the illusory figure surface which had the same luminance at the background. BOLD signals were enhanced at the locations of the surface of the illusory triangle, with the strongest enhancement of activity in the deep layers of V1 (Fig. 6D). Interestingly in this study the laminar BOLD response to a strong visual stimulus was biased towards the superficial layers, as would be expected using GE, however the differences between conditions were strongest in the deeper layers and this difference did not bleed-through into the other layers. This suggests that the problems with GE BOLD may not be so extreme in practice when appropriate comparisons are made between conditions. The laminar profile for top-down activation of visual cortex observed in this study partially agrees with the laminar profile obtained using electrophysiological techniques as described above. One key difference was that the enhanced figure response was confined to the deep layers in the fMRI study, whereas it was also observed in the superficial layers in the electrophysiological study, for figure-ground perception, attention as well as for working memory. One possible explanation for the difference between the studies are signal processing choices. The laminar profiles of top-down effects in the electrophysiological studies described above were obtained after first normalizing the signals to the maximum response of each layer, a procedure that amplifies the weaker signals in the superficial layers. Non-normalized profiles are more biased towards the deep layers, and hence in better agreement with the fMRI results. While we have focused on visual studies here, a recent laminar fMRI study revealed top-down attention effects in the superficial layers of

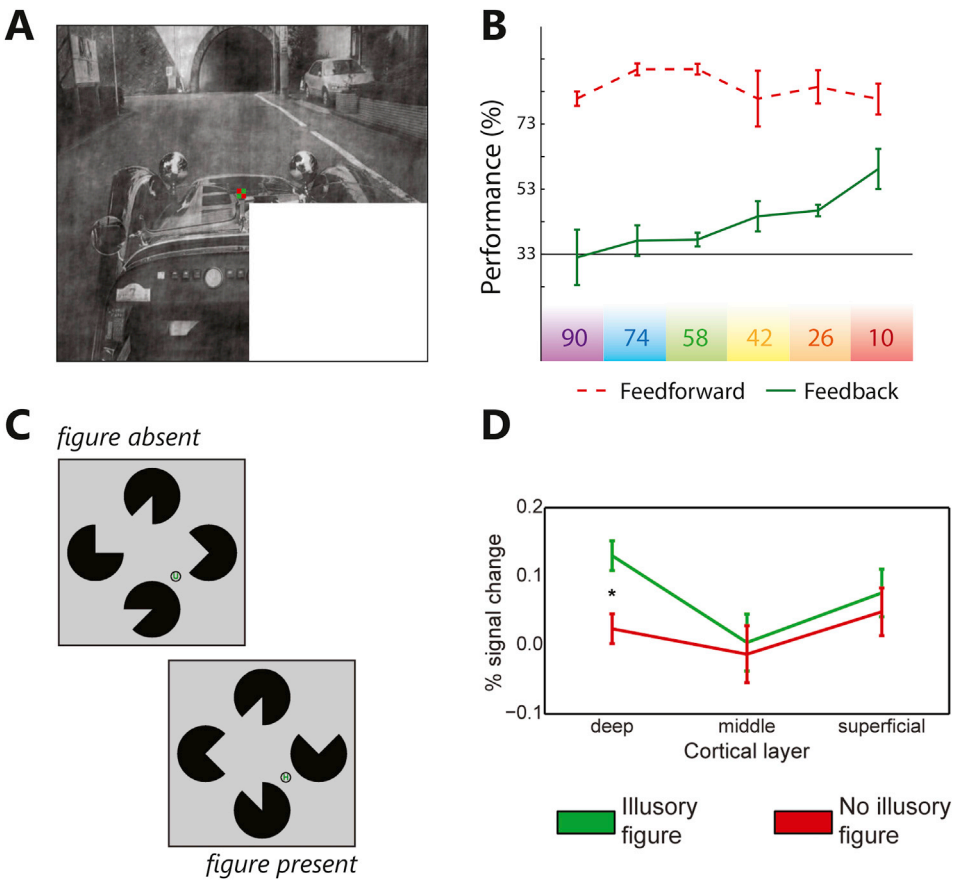

Fig. 6. Results from laminar fMRI studies that examine top-down effects. A) In the study of Muckli et al. (2015) subject saw visual scenes with one region blanked-out. **B)** The identity of the scene could be decoded from BOLD signals in the different layers of V1. For parts of the scene that were stimulated by the image, decoding accuracy was fairly uniform across the layers (red line). For voxels responding to the blanked-out region of the scene (green line), decoding accuracy was significantly stronger in the superficial layers. **C)** In the study of Kok et al. (2016) subjects viewed 'pac-man' elements that either induced the percept of an illusory triangle (bottom image) or were misaligned so that no illusory figure appeared (top image). **D)** BOLD responses from voxels in V1 representing the region of the illusory surface were significantly higher when an illusory surface was present (green line), but only in the deep layers of V1.

primary auditory cortex (A1). Attention to sound did not change overall activity, it but sharpened the frequency tuning in the superficial layers of A1 (De Martino et al., 2015).

In summary, these recent studies suggest that laminar fMRI can reveal top-down effects, which are strongest in the extragranular layers of V1 (i.e. above and below layer 4). While neither study exactly replicated the 'U' shaped profile observed in electrophysiological studies, this may be related to differences in the normalization approaches of the electrophysiological and fMRI studies. Future studies that examine the laminar profile of figure-ground perception, attention and working memory will help to determine if the technical challenges of laminar fMRI can be overcome, revealing the neural computations that take place in the different layers of human visual cortex.

9. Conclusions and outlook

We have reviewed the patterns of spiking and current flow that arise across the different layers of V1 in different visual tasks. The laminar organization of cortex is surprisingly well-preserved across areas, leading to the concept of the canonical cortical micro-circuit, where the idea is that neurons in different areas implement similar neural computations on their inputs (Douglas and Martin, 2004; Gilbert, 1983). However, the question of how well the present findings about laminar profiles will generalize to other cortical areas remains to be answered. The primary visual cortex is a rather unique area with a cell-dense and extended layer 4. At the other end of the cortical spectrum are motor areas with a thin or absent layer 4 and an enlarged layer 5. Studies of the supplementary eye fields (Godlove et al., 2014), which lack a granular layer 4, show some similarities in the pattern of current flow from the middle towards the outer layers, but there are many differences as well (Ninomiya et al., 2015). Within the visual system itself laminar studies have found similarities in the basic processing of visual inputs, but differences in the laminar profile of top-down effects have been reported too (Nandy et al., 2017). Ultimately, further studies of the underlying laminar circuitry in different brain areas of animal models, with the occasional opportunity to record spiking activity from human cortex (Self et al., 2016), will be required to guide the interpretation of laminar fMRI studies.

As MRI technology and analysis techniques now allow access to laminar information it is important to consider the kinds of questions that can be answered with these new and exciting methods, while also appreciating the limitations. The fine temporal resolution of electrophysiological techniques is not available to fMRI scientists so that a separation of feedforward and feedback influences will have to rely on visual stimulation protocols and tasks that can target these different types of activity, as has been elegantly done in the laminar fMRI studies reviewed in the above. It also seems likely that paradigms that use rapidly changing visual stimuli will bias the BOLD signal towards feedforward input and increase activity in the middle layers, while those that use slower stimuli, which diminish the contribution of transients to the signal, will emphasize the contribution of the superficial and deep layers. One laminar MRI study in humans that compared rapidly and slowly changing stimuli appears to bear out this prediction (Olman et al., 2012).

The great advantage of laminar fMRI is that it can be applied to humans, opening up the possibility of studying the role of the different

layers in more complex tasks and phenomenon that are not accessible, or extremely difficult to study, in monkeys. For example, the study of visual imagery is not possible in animals. The use of laminar fMRI to understand how top-down projections activate different layers in different brain areas would help to advance our understanding of this phenomenon. The link between the BOLD signal and synaptic activity may make laminar fMRI more sensitive to the signals carried by feedback connections than invasive electrophysiological measures. This has been observed in studies of attention and binocular rivalry in which the BOLD signal modulations are much greater in magnitude than the modulations of spiking activity (Maier et al., 2008; Ress et al., 2000; Tong and Engel, 2001). Hence, laminar fMRI may become a powerful tool to study the functions of the feedback connections, once the relationship between laminar fMRI and synaptic and spiking activity becomes clearer. Feedback connections in the visual system play a critical role in integrating the bottom-up sensory evidence coming from the retina with top-down information about visual context (Lamme and Roelfsema, 2000), current sensory hypotheses (Nienborg and Roelfsema, 2015), and behavioral relevance (Stanisor et al., 2013). Yet, a lot remains to be learned about the interactions between bottom-up and top-down signals into a cortical area. We expect that a deeper understanding of the processing in the different cortical layers will help to arbitrate between contrasting theories about the influence of top-down influences on a cortical column (Friston, 2010; Lee and Mumford, 2003; Nienborg and Roelfsema, 2015; Rao and Ballard, 1999). Laminar fMRI studies may therefore provide an important bridge between human studies and invasive experiments in animal models that aim to test these theories.

Acknowledgements

We are grateful to Alessio Fracasso, Serge Dumoulin, Lucy Petro, Lars Muckli, Peter Kok and Floris de Lange for their assistance in providing figures for this review. PRR was supported by NWO (ALW grant 823-02-010; MaGW grant 400-09-198 and Natural Artificial Intelligence grant 656-000-002) and the EU (Marie-Curie Action PITN-GA-2011-290011, ERC advanced grant #339490 “Cortic_al_gorithms”, the Human Brain Project, agreement no. 720270).

References

Anderson, J.C., Martin, K.A., 2009. The synaptic connections between cortical areas V1 and V2 in macaque monkey. J. Neurosci. 29, 11283–11293.
Attwell, D., Iadecola, C., 2002. The neural basis of functional brain imaging signals. Trends Neurosci. 25, 621–625.
Benevento, L.A., Rezak, M., 1976. The cortical projections of the inferior pulvinar and adjacent lateral pulvinar in the rhesus monkey (Macaca mulatta): an autoradiographic study. Brain Res. 108, 1–24.
Benevento, L.A., Rezak, M., 1975. Extrageniculate projections to layers VI and I of striate cortex (area 17) in the rhesus monkey (Macaca mulatta). Brain Res. 96, 51–55.
Berens, P., Keliris, G.A., Ecker, A.S., Logothetis, N.K., Tolias, A.S., 2008. Comparing the feature selectivity of the gamma-band of the local field potential and the underlying spiking activity in primate visual cortex. Front. Syst. Neurosci. 2, 2.
Binzegger, T., Douglas, R.J., Martin, K.A., 2004. A quantitative map of the circuit of cat primary visual cortex. J. Neurosci. 24, 8441–8453.
Blasdel, G.G., Lund, J.S., 1983. Termination of afferent axons in macaque striate cortex. J. Neurosci. 3, 1389–1413.
Busse, L., Ayaz, A., Dhruv, N.T., Katzner, S., Saleem, A.B., Schölvinck, M.L., Zaharia, A.D., Carandini, M., 2011. The detection of visual contrast in the behaving mouse. J. Neurosci. 31, 11351–11361.
Buzsáki, G., Anastassiou, C.A., Koch, C., 2012. The origin of extracellular fields and currents — EEG, ECoG, LFP and spikes. Nat. Rev. Neurosci. 13, 407–420.
Callaway, E.M., 2004. Close encounters: how cortical neurons find and connect to their correct synaptic partners depends on the cell type. Neuron 43, 156–158.
Chen, G., Wang, F., Gore, J.C., Roe, A.W., 2013. Layer-specific BOLD activation in awake monkey V1 revealed by ultra-high spatial resolution functional magnetic resonance imaging. Neuroimage 64, 147–155.
De Martino, F., Moerel, M., Ugurbil, K., Goebel, R., Yacoub, E., Formisano, E., 2015. Frequency preference and attention effects across cortical depths in the human primary auditory cortex. Proc. Natl. Acad. Sci. 112, 16036–16041.
De Martino, F., Zimmermann, J., Muckli, L., Ugurbil, K., Yacoub, E., Goebel, R., 2013. Cortical depth dependent functional responses in humans at 7T: improved specificity with 3D GRASE. PLoS One 8, e60514.
Douglas, R.J., Martin, K.A., 2004. Neuronal circuits of the neocortex. Annu. Rev. Neurosci. 27, 419–451.
Duvernoy, H.M., Delon, S., Vannson, J.L., 1981. Cortical blood vessels of the human brain. Brain Res. Bull. 7, 519–579.
Engel, S.A., Rumelhart, D.E., Wandell, B.A., Lee, A.T., Glover, G.H., Chichilnisky, E.J., Shadlen, M.N., 1994. fMRI of human visual cortex. Nature 369, 525.
Felleman, D.J., Van Essen, D.C., 1991. Distributed hierarchical processing in the primate cerebral cortex. Cereb. Cortex 1, 1–47.
Fracasso, A., Petridou, N., Dumoulin, S.O., 2016. Systematic variation of population receptive field properties across cortical depth in human visual cortex. Neuroimage 139, 427–438.
Friston, K., 2010. The free-energy principle: a unified brain theory? Nat. Rev. Neurosci. 11, 127–138.
Gambino, F., Pagès, S., Kehayas, V., Baptista, D., Tatti, R., Carleton, A., Holtmaat, A., 2014. Sensory-evoked LTP driven by dendritic plateau potentials in vivo. Nature 515, 116–119.
Gilbert, C.D., 1983. Microcircuitry of the visual cortex. Annu. Rev. Neurosci. 6, 217–247.
Gilbert, C.D., 1977. Laminar differences in receptive field properties of cells in cat primary visual cortex. J. Physiol. 268, 391–421.
Godlove, D.C., Maier, A., Woodman, G.F., Schall, J.D., 2014. Microcircuitry of agranular frontal cortex: testing the generality of the canonical cortical microcircuit. J. Neurosci. 34, 5355–5369.
Goense, J.B., Logothetis, N.K., 2008. Neurophysiology of the BOLD fMRI signal in awake monkeys. Curr. Biol. 18, 631–640.
Goense, J.B., Logothetis, N.K., 2006. Laminar specificity in monkey V1 using high-resolution SE-fMRI. Magn. Reson. Imaging 24, 381–392.
Hendrickson, A.E., Wilson, J.R., Ogren, M.P., 1978. The neuroanatomical organization of pathways between the dorsal lateral geniculate nucleus and visual cortex in Old World and New World primates. J. Comp. Neurol. 182, 123–136.
Horton, J.C., Hubel, D.H., 1981. Regular patchy distribution of cytochrome oxidase staining in primary visual cortex of macaque monkey. Nature 292, 762–764.
Houtkamp, R., Spekreijse, H., Roelfsema, P.R., 2003. A gradual spread of attention during mental curve tracing. Percept. Psychophys. 65, 1136–1144.
Hubel, D.H., Wiesel, T.N., 1977. Ferrier lecture. Functional architecture of macaque monkey visual cortex. Proc. R. Soc. Lond. B. Biol. Sci. 198, 1–59.
Hubel, D.H., Wiesel, T.N., 1969. Anatomical demonstration of columns in the monkey striate cortex. Nature 221, 747–750.
Hubel, D.H., Wiesel, T.N., 1968. Receptive fields and functional architecture of monkey striate cortex. J. Physiol. 195, 215–243.
Hubel, D.H., Wiesel, T.N., 1962. Receptive fields, binocular interaction and functional architecture in the cat's visual cortex. J. Physiol. 160, 106–154, 2.
Kajikawa, Y., Schroeder, C.E., 2011. How local is the local field potential? Neuron 72, 847–858.
Kemper, V.G., De Martino, F., Emmerling, T.C., Yacoub, E., Goebel, R., 2017. High resolution data analysis strategies for mesoscale human functional MRI at 7 and 9.4 T. Neuroimage.
Kennedy, C., Des Rosiers, M.H., Sakurada, O., Shinohara, M., Reivich, M., Jehle, J.W., Sokoloff, L., 1976. Metabolic mapping of the primary visual system of the monkey by means of the autoradiographic [14C]deoxyglucose technique. Proc. Natl. Acad. Sci. U. S. A. 73, 4230–4234.
Klein, C., Evrard, H.C., Shapcott, K.A., Haverkamp, S., Logothetis, N.K., Schmid, M.C., 2016. Cell-targeted optogenetics and electrical microstimulation reveal the primate koniocellular projection to supra-granular visual cortex. Neuron 90, 143–151.
Kok, P., Bains, L.J., van Mourik, T., Norris, D.G., de Lange, F.P., 2016. Selective activation of the deep layers of the human primary visual cortex by top-down feedback. Curr. Biol. 26, 371–376.
Koopmans, P.J., Barth, M., Norris, D.G., 2010. Layer-specific BOLD activation in human V1. Hum. Brain Mapp. 31, 1297–1304.
Lamme, V.A., 1995. The neurophysiology visual cortex figure-ground segregation primary. J. Neurosci. 15, 1605–1615.
Lamme, V.A., Roelfsema, P.R., 2000. The distinct modes of vision offered by feedforward and recurrent processing. Trends Neurosci. 23, 571–579.
Lamme, V.A., Zipser, K., Spekreijse, H., 1998. Figure-ground activity in primary visual cortex is suppressed by anesthesia. Proc. Natl. Acad. Sci. U. S. A. 95, 3263–3268.
Lauritzen, M., 2005. Reading vascular changes in brain imaging: is dendritic calcium the key? Nat. Rev. Neurosci. 6, 77–85.
Lee, T.S., Mumford, D., 2003. Hierarchical Bayesian inference in the visual cortex. J. Opt. Soc. Am. A. Opt. Image Sci. Vis. 20, 1434–1448.
Livingstone, M.S., Hubel, D.H., 1984. Anatomy and physiology of a color system in the primate visual cortex. J. Neurosci. 4, 309–356.
Logothetis, N.K., 2008. What we can do and what we cannot do with fMRI. Nature 453, 869–878.
Logothetis, N.K., Pauls, J., Augath, M., Trinath, T., Oeltermann, A., 2001. Neurophysiological investigation of the basis of the fMRI signal. Nature 412, 150–157.
Lund, J.S., 1988. Anatomical organization of macaque monkey striate visual cortex. Annu. Rev. Neurosci. 11, 253–288.
Maier, A., Aura, C.J., Leopold, D.A., 2011. Infragranular sources of sustained local field potential responses in macaque primary visual cortex. J. Neurosci. 31, 1971–1980.
Maier, A., Wilke, M., Aura, C., Zhu, C., Ye, F.Q., Leopold, D.A., 2008. Divergence of fMRI and neural signals in V1 during perceptual suppression in the awake monkey. Nat. Neurosci. 11, 1193–1200.
Markov, N.T., Ercsey-Ravasz, M.M., Ribeiro Gomes, A.R., Lamy, C., Magrou, L., Vezoli, J., Misery, P., Falchier, A., Quilodran, R., Gariel, M.A., Sallet, J., Gamanut, R., Huissoud, C., Clavagnier, S., Giroud, P., Sappey-Marinier, D., Barone, P., Dehay, C., Toroczkai, Z., Knoblauch, K., Van Essen, D.C., Kennedy, H., 2014. A weighted and directed interareal connectivity matrix for macaque cerebral cortex. Cereb. Cortex 24, 17–36.

Maunsell, J.H., van Essen, D.C., 1983. The connections of the middle temporal visual area (MT) and their relationship to a cortical hierarchy in the macaque monkey. J. Neurosci. 3, 2563–2586.
Mehta, A.D., Ulbert, I., Schroeder, C.E., 2000. Intermodal selective attention in monkeys. II: physiological mechanisms of modulation. Cereb. Cortex 10, 359–370.
Mitzdorf, U., 1985. Current source-density method and application in cat cerebral cortex: investigation of evoked potentials and EEG phenomena. Physiol. Rev. 65, 37–100.
Muckli, L., De Martino, F., Vizioli, L., Petro, L.S., Smith, F.W., Ugurbil, K., Goebel, R., Yacoub, E., 2015. Contextual feedback to superficial layers of V1. Curr. Biol. 1–6.
Mukamel, R., Gelbard, H., Arieli, A., Hasson, U., Fried, I., Malach, R., 2005. Coupling between neuronal firing, field potentials, and FMRI in human auditory cortex. Science 309, 951–954.
Nandy, A.S., Nassi, J.J., Reynolds, J.H., 2017. Laminar organization of attentional modulation in macaque visual area V4. Neuron 93, 235–246.
Nicholson, C., Freeman, J.A., 1975. Theory of current source-density analysis and determination of conductivity tensor for anuran cerebellum. J. Neurophysiol. 38, 356–368.
Nienborg, H., Roelfsema, P.R., 2015. Belief states as a framework to explain extra-retinal influences in visual cortex. Curr. Opin. Neurobiol. 32, 45–52.
Ninomiya, T., Dougherty, K., Godlove, D.C., Schall, J.D., Maier, A., 2015. Microcircuitry of agranular frontal cortex: contrasting laminar connectivity between occipital and frontal areas. J. Neurophysiol. 113, 3242–3255.
O'Herron, P., Chhatbar, P.Y., Levy, M., Shen, Z., Schramm, A.E., Lu, Z., Kara, P., 2016. Neural correlates of single-vessel haemodynamic responses in vivo. Nature 534, 378–382.
Ogren, M.P., Hendrickson, A.E., 1977. The distribution of pulvinar terminals in visual areas 17 and 18 of the monkey. Brain Res. 137, 343–350.
Olman, C.A., Harel, N., Feinberg, D.A., He, S., Zhang, P., Ugurbil, K., Yacoub, E., 2012. Layer-specific fMRI reflects different neuronal computations at different depths in human V1. PLoS One 7, e32536.
Pooresmaeili, A., Roelfsema, P.R., 2014. A growth-cone model for the spread of object-based attention during contour grouping. Curr. Biol. 24, 2869–2877.
Poort, J., Raudies, F., Wannig, A., Lamme, V.A., Neumann, H., Roelfsema, P.R., 2012. The role of attention in figure-ground segregation in areas V1 and V4 of the visual cortex. Neuron 75, 143–156.
Poort, J., Self, M.W., van Vugt, B., Malkki, H., Roelfsema, P.R., 2016. Texture segregation causes early figure enhancement and later ground suppression in areas V1 and V4 of visual cortex. Cereb. Cortex 26, 3964–3976.
Rao, R.P., Ballard, D.H., 1999. Predictive coding in the visual cortex: a functional interpretation of some extra-classical receptive-field effects. Nat. Neurosci. 2, 79–87.
Ress, D., Backus, B.T., Heeger, D.J., 2000. Activity in primary visual cortex predicts performance in a visual detection task. Nat. Neurosci. 3, 940–945.
Ringach, D.L., Shapley, R.M., Hawken, M.J., 2002. Orientation selectivity in macaque V1: diversity and laminar dependence. J. Neurosci. 22, 5639–5651.
Rockland, K.S., Pandya, D.N., 1979. Laminar origins and terminations of cortical connections of the occipital lobe in the rhesus monkey. Brain Res. 179, 3–20.
Rockland, K.S., Virga, A., 1989. Terminal arbors of individual "feedback" axons projecting from area V2 to V1 in the macaque monkey: a study using immunohistochemistry of anterogradely transported Phaseolus vulgaris-leucoagglutinin. J. Comp. Neurol. 285, 54–72.
Roelfsema, P.R., 2006. Cortical algorithms for perceptual grouping. Annu. Rev. Neurosci. 29, 203–227.
Roelfsema, P.R., Lamme, V.A., Spekreijse, H., 1998. Object-based attention in the primary visual cortex of the macaque monkey. Nature 395, 376–381.
Salin, P.A., Bullier, J., 1995. Corticocortical connections in the visual system: structure and function. Physiol. Rev. 75, 107–154.
Sceniak, M.P., Hawken, M.J., Shapley, R., 2001. Visual spatial characterization of macaque V1 neurons. J. Neurophysiol. 85, 1873–1887.
Schiller, P.H., Finlay, B.L., Volman, S.F., 1976. Quantitative studies of single-cell properties in monkey striate cortex. III. Spatial frequency. J. Neurophysiol. 39, 1334–1351.
Scholte, H.S., Spekreijse, H., Roelfsema, P.R., 2001. The spatial profile of visual attention in mental curve tracing. Vis. Res. 41, 2569–2580.
Schroeder, C.E., Mehta, A.D., Givre, S.J., 1998. A spatiotemporal profile of visual system activation revealed by current source density analysis in the awake macaque. Cereb. Cortex 8, 575–592.
Schroeder, C.E., Tenke, C.E., Givre, S.J., Arezzo, J.C., Vaughan, H.G., 1991. Striate cortical contribution to the surface-recorded pattern-reversal VEP in the alert monkey. Vis. Res. 31, 1143–1157.
Self, M.W., Kooijmans, R.N., Supèr, H., Lamme, V.A., Roelfsema, P.R., 2012. Different glutamate receptors convey feedforward and recurrent processing in macaque V1. Proc. Natl. Acad. Sci. 109, 11031–11036.
Self, M.W., Peters, J.C., Possel, J.K., Reithler, J., Goebel, R., Ris, P., Jeurissen, D., Reddy, L., Claus, S., Baayen, J.C., Roelfsema, P.R., 2016. The effects of context and attention on spiking activity in human early visual cortex. PLoS Biol. 14, e1002420.
Self, M.W., van Kerkoerle, T., Supèr, H., Roelfsema, P.R., 2013. Distinct roles of the cortical layers of area V1 in figure-ground segregation. Curr. Biol. 23, 2121–2129.
Sherman, S.M., 2016. Thalamus plays a central role in ongoing cortical functioning. Nat. Neurosci. 19, 533–541.
Shipp, S., 2003. The functional logic of cortico-pulvinar connections. Philos. Trans. R. Soc. Lond. B. Biol. Sci. 358, 1605–1624.
Smith, F.W., Muckli, L., 2010. Nonstimulated early visual areas carry information about surrounding context. Proc. Natl. Acad. Sci. 107, 20099–20103.
Snodderly, D.M., Gur, M., 1995. Organization of striate cortex of alert, trained monkeys (Macaca fascicularis): ongoing activity, stimulus selectivity, and widths of receptive field activating regions. J. Neurophysiol. 74, 2100–2125.
Stanisor, L., van der Togt, C., Pennartz, C.M., Roelfsema, P.R., 2013. A unified selection signal for attention and reward in primary visual cortex. Proc. Natl. Acad. Sci. 110, 9136–9141.
Supèr, H., Roelfsema, P.R., 2005. Chronic multiunit recordings in behaving animals: advantages and limitations. Prog. Brain Res. 147, 263–282.
Tong, F., Engel, S.A., 2001. Interocular rivalry revealed in the human cortical blind-spot representation. Nature 411, 195–199.
Tootell, R.B., Hamilton, S.L., Silverman, M.S., Switkes, E., 1988a. Functional anatomy of macaque striate cortex. I. Ocular dominance, binocular interactions, and baseline conditions. J. Neurosci. 8, 1500–1530.
Tootell, R.B., Switkes, E., Silverman, M.S., Hamilton, S.L., 1988b. Functional anatomy of macaque striate cortex. II. Retinotopic organization. J. Neurosci. 8, 1531–1568.
van Kerkoerle, T., Self, M.W., Dagnino, B., Gariel-Mathis, M.A., Poort, J., van der Togt, C., Roelfsema, P.R., 2014. Alpha and gamma oscillations characterize feedback and feedforward processing in monkey visual cortex. Proc. Natl. Acad. Sci. U. S. A. 111.
van Kerkoerle, T., Self, M.W., Roelfsema, P.R., 2017. Layer-specificity in the effects of attention and working memory on activity in primary visual cortex. Nat. Commun. 8, 13804.
Vanduffel, W., Tootell, R.B., Orban, G.A., 2000. Attention-dependent suppression of metabolic activity in the early stages of the macaque visual system. Cereb. Cortex 10, 109–126.
Wandell, B.A., Dumoulin, S.O., Brewer, A.A., 2007. Visual field maps in human cortex. Neuron 56, 366–383.
Weber, B., Keller, A.L., Reichold, J., Logothetis, N.K., 2008. The microvascular system of the striate and extrastriate visual cortex of the macaque. Cereb. Cortex 18, 2318–2330.
Wilke, M., Logothetis, N.K., Leopold, D.A., 2006. Local field potential reflects perceptual suppression in monkey visual cortex. Proc. Natl. Acad. Sci. U. S. A. 103, 17507–17512.
Wong-Riley, M., 1979. Changes in the visual system of monocularly sutured or enucleated cats demonstrable with cytochrome oxidase histochemistry. Brain Res. 171, 11–28.
Xing, D., Yeh, C.-I., Burns, S., Shapley, R.M., 2012. Laminar analysis of visually evoked activity in the primary visual cortex. Proc. Natl. Acad. Sci. U. S. A. 109, 13871–13876.
Xing, D., Yeh, C.-I., Gordon, J., Shapley, R.M., 2014. Cortical brightness adaptation when darkness and brightness produce different dynamical states in the visual cortex. Proc. Natl. Acad. Sci. U. S. A. 111, 1210–1215.
Xing, D., Yeh, C.-I., Shapley, R.M., 2009. Spatial spread of the local field potential and its laminar variation in visual cortex. J. Neurosci. 29, 11540–11549.
Zimmermann, J., Goebel, R., De Martino, F., van de Moortele, P.-F., Feinberg, D., Adriany, G., Chaimow, D., Shmuel, A., Uğurbil, K., Yacoub, E., 2011. Mapping the organization of Axis of motion selective features in human area MT using high-field fMRI. PLoS One 6, e28716.